

Lipid Nanoparticles for *In Vivo* Lung Delivery of CRISPR-Cas9 Ribonucleoproteins Allow Gene Editing of Clinical Targets

Rebecca M. Haley, Marshall S. Padilla, Rakan D. El-Mayta, Ryann A. Joseph, Jesse A. Weber, Christian G. Figueroa-Espada, Alvin J. Mukalel, Adele S. Ricciardi, Rohan Palanki, Hannah C. Geisler, Matthew T. Jester, Beverly L. Davidson, and Michael J. Mitchell*



Cite This: *ACS Nano* 2025, 19, 13790–13804



Read Online

ACCESS |



Metrics & More



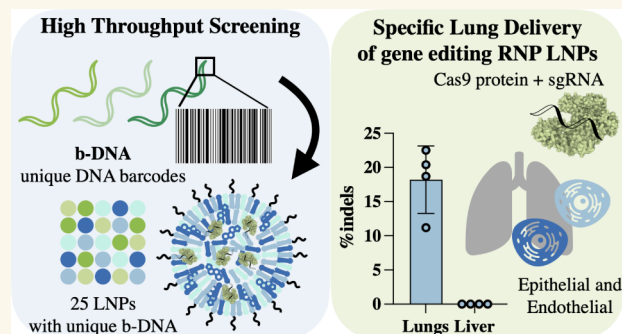
Article Recommendations



Supporting Information

ABSTRACT: In the past 10 years, CRISPR-Cas9 has revolutionized the gene-editing field due to its modularity, simplicity, and efficacy. It has been applied for the creation of *in vivo* models, to further understand human biology, and toward the curing of genetic diseases. However, there remain significant delivery barriers for CRISPR-Cas9 application in the clinic, especially for *in vivo* and extrahepatic applications. In this work, high-throughput molecular barcoding techniques were used alongside traditional screening methodologies to simultaneously evaluate LNP formulations encapsulating ribonucleoproteins (RNPs) for *in vitro* gene-editing efficiency and *in vivo* biodistribution. This resulted in the identification of a lung-tropic LNP formulation, which shows efficient gene editing in endothelial and epithelial cells within the lung, targeting both model reporter and clinically relevant genomic targets. Further, this LNP shows no off-target indel formation in the liver, making it a highly specific extrahepatic delivery system for lung-editing applications.

KEYWORDS: lipid nanoparticle, drug delivery, DNA barcoding, high-throughput screening, gene editing, ribonucleoprotein, extrahepatic



In 2013, the CRISPR-Cas9 system was successfully applied for gene editing in cells,^{1–5} 25 years after clustered regularly interspaced short palindromic repeats (CRISPR) was first discovered in the DNA of *Escherichia coli* bacteria.⁶ Today, CRISPR-Cas9 is the most widely used genome editor⁷ and has been used to create *in vitro* and *in vivo* research models and identify biological pathways using CRISPR screens and has begun to see clinical application with the recent FDA approval of Casgevy, a CRISPR-Cas9-based approach for sickle cell treatment.

In bacterial cells, the type II CRISPR-Cas system is used as a form of adaptive immunity against viruses and plasmids. Cas9—a specific endonuclease associated with CRISPR—complexes with tracrRNA, a binding scaffold for the protein. This, in turn, interacts with an RNA guide sequence (crRNA) that is complementary to a DNA target locus. In this fashion, Cas9 can induce a double-stranded DNA break at a site-specific location. When this occurs in eukaryotic cells, DNA repair pathways are activated. Nonhomologous end joining (NHEJ)—the most common repair pathway—often results in the creation of insertion or deletion mutations (indels) at the

cut site. When utilized by bacterial cells, this causes mutation of infecting viral material to the point of nonfunction. However, this can be leveraged to knockout a gene of interest in eukaryotic cells, making CRISPR-Cas9 a simple system for powerful gene editing.

Currently, crRNA and tracrRNA are commonly combined into a single-guide RNA (sgRNA) that both pairs with DNA and binds to Cas9. Together, the complexed Cas9 protein and sgRNA form a ribonucleoprotein (RNP) that serves as a single functional unit for DNA targeting and cutting. RNPs can be delivered to cells for knockout applications or with the addition of a DNA repair template (typically single-stranded DNA, ssDNA). If a DNA template is present, cells can undergo homology-directed repair (HDR), which incorporates the

Received: November 19, 2024

Revised: March 20, 2025

Accepted: March 21, 2025

Published: April 4, 2025



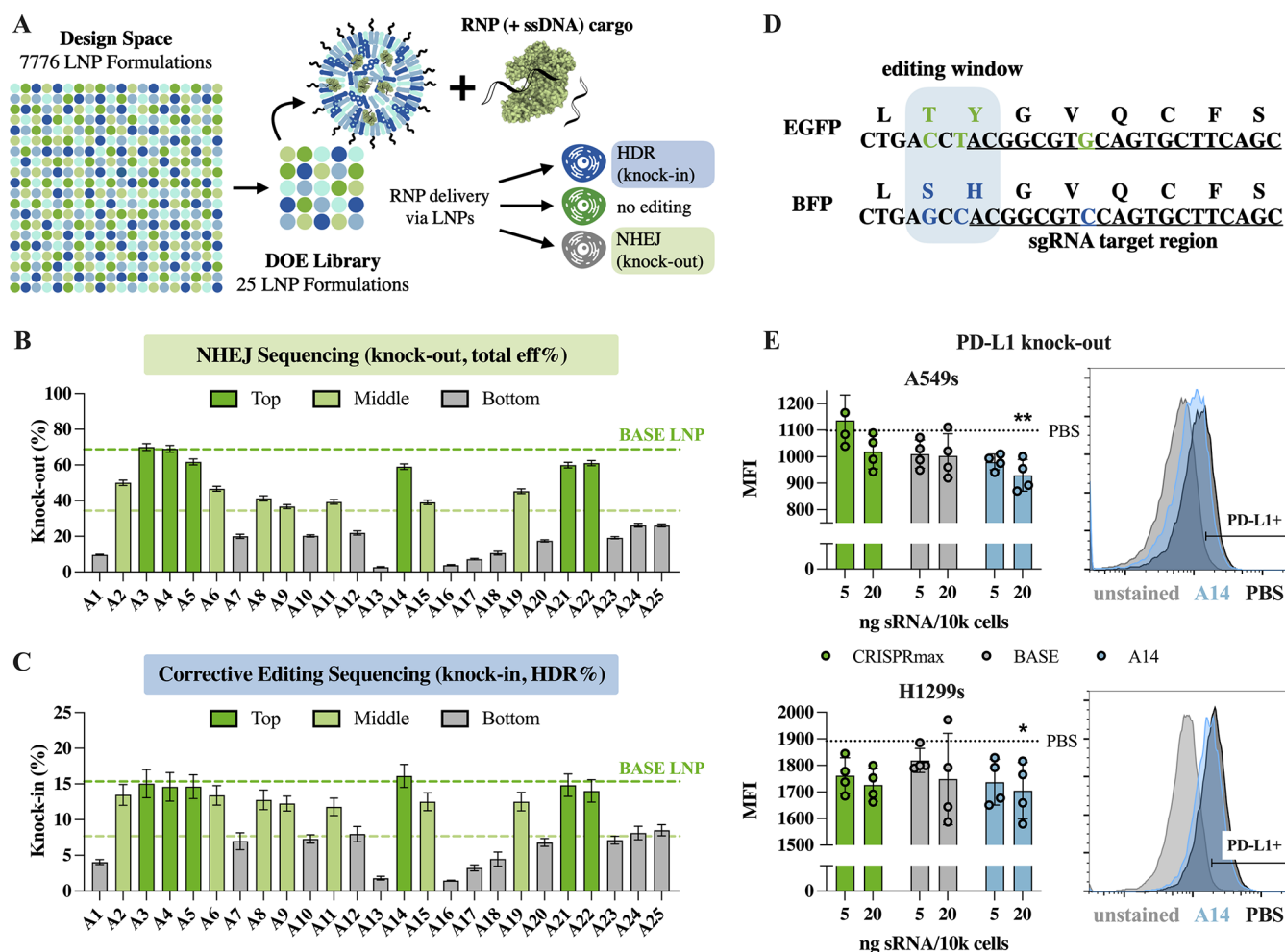


Figure 2. Optimizing LNP excipient components for RNP and ssDNA delivery—and resulting knock-in editing—using a design of experiment (DOE) approach. (A) DOE allows for a design space of 7776 LNPs to be analyzed by testing only 25 LNPs. These LNPs encapsulate RNPs with single guide RNA (sgRNA) targeting EGFP and single stranded donor DNA (ssDNA) to change the EGFP fluorophore to BFP. (B) Of the 25 LNPs tested, six were identified as hits in H1299 cells, having similar knockout efficiencies (indel formation, based on sanger sequencing data and TIDER analysis) to the base formulation tested. Seven more were identified as middle performers. $n = 3$. (C) The same top and middle performers were identified when looking at knock-in efficiencies (homology directed repair, HDR); $n = 3$. (D) EGFP and BFP nucleic acid and amino acid sequences at the site of interest, which determines fluorophore color. EGFP and BFP are very similar fluorophores, with only two base pair and two amino acid changes within the editing window. (E) PD-L1 knockout was tested with the top performing formulation, A14, alongside control delivery vectors in both H1299 and A549 cells. Only A14 showed a significant reduction in PD-L1 signal, compared to the untreated cell control; $n = 4$. *: $p < 0.05$ and **: $p < 0.01$. Error bars show SD.

the cell. By delivering the RNP complex, many limitations of current approaches can be mitigated. With respect to toxicity, RNPs are thought to cause lower levels of TLR activation and have minimal risk of off-target effects as they degrade quickly after functioning in the cell.²⁶ RNPs have also shown high editing efficiencies and improved stability when compared with their mRNA counterparts, and this improvement in editing is likely due in part to the kinetic advantages of delivering the whole functional unit. In contrast, mRNA/sgRNA delivery results in a race for mRNA expression before sgRNA degradation and is more wasteful in terms of the amount of sgRNA delivered per cell.

RNP delivery is a recent but quickly growing field. Similar to mRNA delivery, lipid,^{17,18,25,28,29} polymer,³⁰ and inorganic^{31,32} nanoparticle systems have all been shown to encapsulate and deliver RNPs intracellularly. However, LNPs have emerged as an especially promising delivery vector due to their previous FDA approval^{33–35}—which comes with a focus on large-scale

manufacturing³⁶ and clinical safety—as well as their high level of modularity. While LNPs are more widely used for mRNA and small interfering RNA (siRNA) delivery applications,^{37–39} their recent utilization for intracellular protein delivery—both in the gene editing field and beyond^{40–42}—makes them an ideal candidate for RNP delivery.

However, while protein delivery with LNPs has been achieved, it remains relatively unexplored, especially in applications that require extrahepatic delivery. As LNPs typically distribute to the liver *in vivo*, there is particular interest in the development of systems that can reach alternative organs and cell subtypes. Targeting is also highly desirable, considering the potential severity of off-target effects. While CRISPR-Cas9 is site-specific by design, there is always concern about off-target or unintended-target editing, and precise delivery technologies will allow for the commercialization of this editing platform.

To help overcome these limitations, we aimed to develop LNP formulations, which can codeliver the Cas9 protein, sgRNA, and donor ssDNA for efficient gene editing *in vitro* and *in vivo* to extrahepatic targets, specifically the lungs. To achieve these goals, we first screened different ionizable lipid structures for RNP delivery *in vitro*. Top-performing lipids were moved forward to a design of experiments (DOE) screen, which allowed a large LNP formulation space to be evaluated with only 25 representative LNPs. This 25-LNP library was screened *in vitro* to identify formulation parameters that result in efficient intracellular delivery and gene editing, as well as *in vivo*—utilizing a high-throughput molecular barcoding approach—to identify parameters that influence LNP distribution and can result in efficient extrahepatic delivery. Combining the results from both *in vitro* and *in vivo* screens, we further evaluated LNP formulations of interest for corrective editing *in vitro* and lung-specific editing *in vivo*.

Ultimately, this work resulted in the identification of a highly lung-specific LNP formulation for delivery of the Cas9 protein. This formulation can deliver RNPs to both endothelial and epithelial cells within the lung and targets native genomic loci with no off-target liver editing. In summary, this work shows LNPs that perform at a more clinically translatable level and may inform future RNP delivery work by highlighting factors that influence both high knock-in efficiencies and favorable biodistributions.

RESULTS AND DISCUSSION

While CRISPR-Cas9 editing machinery has been delivered by LNPs in the past, much of the existing work focuses on the encapsulation and delivery of mRNA, which encodes for the Cas9 protein,^{14,17–22} as opposed to the delivery of the RNP complex as a single unit. LNP-based delivery of the Cas9 protein has been published with the usage of the commercially available lipid C12–200.²⁵ Therefore, as a control for this work, this previously published formulation was used as a base LNP control (Figure S1) and as a foundation for additional improvement in both gene-editing efficiency and *in vivo* distribution.

Design of RNP-Encapsulating LNPs and Initial Ionizable Lipid Screen. A previously designed library of ionizable lipids⁴³—based on the same C12–200 lipid—has been used for successful protein delivery in the past.⁴² Therefore, this same lipid library was screened for the encapsulation and *in vitro* delivery of the RNP complex (Figure 1A). Taking inspiration from previous protein delivery work,^{42,44,45} as well as published RNP delivery literature,^{17,18,25,29} the positively charged lipid DOTAP was included as a fifth component in the LNP system to overcome the nonideal charge balance of the RNP complex, which is negatively charged overall due to the sgRNA but has regions of positive and neutral charge on the Cas9 surface. The five LNP lipid components—ionizable lipid, DOTAP, neutral helper lipid DOPE, cholesterol, and lipid-anchored PEG—are combined in an ethanol phase, while the Cas9 protein and sgRNA are combined in an aqueous phase of PBS—instead of the traditional citrate buffer—to complex and form the RNP. This change of buffer was made due to previous work, which showed negative effects when using citrate buffer with protein cargo^{18,42} and a preliminary screen of alternative aqueous buffers (Figure S2). These two phases are then mixed using a microfluidic device to form LNPs³⁶ (Figure 1B).

To start, sgRNA was used to target EGFP to evaluate intracellular delivery and gene editing efficiency via EGFP knockout, caused by NHEJ and indel formation. All LNPs in this library were characterized for size, PDI, surface zeta potential, and protein concentration (Figure 1). Interestingly, all but one of the C16 lipids tested caused the formation of large or aggregated particles (Figure S1A), which showed poor RNP encapsulation and resulting Cas9 protein concentration (Figure S1B). For this initial screen, EGFP knockout was evaluated in H1299 cells via fluorescence as measured by flow cytometry. The H1299 cell line is an epithelial-like lung cancer line, which has been modified to express EGFP. From the 24 initial 24 ionizable lipids tested, four were identified as top performers (C12–5, C14–2, C14–5, and C14–7, Figure 1C,D) and were moved forward to additional testing.

A Design of Experiments LNP Library to Evaluate In Vitro Editing Efficiency. Once LNPs were identified that could successfully edit cells *in vitro*, a larger screen was formulated using a design of experiments (DOE) approach (Figure 2A). This allows a large design space—in this case, 7776 LNP formulations—to be represented by a smaller 25 LNP library. This library focused on changing the lipid excipient ratios to optimize LNPs not only for RNP delivery but also for the encapsulation and delivery of donor ssDNA templates as a third cargo for corrective knock-in applications. In this context, LNP excipients are the lipid-based components found in the ethanol phase—the ionizable lipid, cationic lipid, neutral helper lipid, cholesterol, and lipid-anchored PEG—and all excipients except cholesterol (which was held at a molar ratio of 30) were each tested at five different molar ratios. Additionally, five ionizable lipid structures were tested (C12–200, C12–5, C14–2, C14–5, and C14–7), and five protein-to-lipid ratios were tested for a total of six variables, each under five different conditions (6⁵ formulations, Table S1). As before, these LNPs were evaluated for size, PDI, and surface zeta potential (Figure S3A). As these LNPs contain both sgRNA and ssDNA, respective encapsulation and concentrations of RNA and DNA were evaluated as well (Figure S3B).

For this larger library screen, an EGFP-to-BFP editing model^{46,47} was used to evaluate gene editing, and Sanger sequencing was used to identify knockout (indels formed by NHEJ) and knock-in (BFP edits formed by HDR) efficiencies. In this model, cells with no editing retain EGFP expression, while cells that undergo NHEJ have no fluorescence. Cells that undergo HDR exhibit BFP expression and fluorescence. As EGFP and BFP are very similar fluorophores, with only two base pair and two amino acid changes causing a change in fluorescence (Figure 2D), this model mimics Mendelian diseases with very small or single mutations.

From this screen, six formulations (A3, A4, A5, A14, A21, and A22) were identified as hits, having knockout efficiencies (indel formation, based on Sanger sequencing data and TIDER analysis) similar to those of the base formulation tested. Seven more formulations were identified as middle performers, with reduced but still functional levels of intracellular delivery and gene editing. The top-performing LNP formulation, A14, based on corrective editing sequencing, was additionally tested alongside the CRISPRmax commercial control and base LNP for PD-L1 knockout. This confirmed that editing efficiencies were such that differences could be seen with a clinical target as opposed to a model fluorophore. In both A549 and H1299 cells, only the A14 formulation (at 20 ng sgRNA/10 000 cells) resulted in a significant decrease in PD-L1 signal, compared to

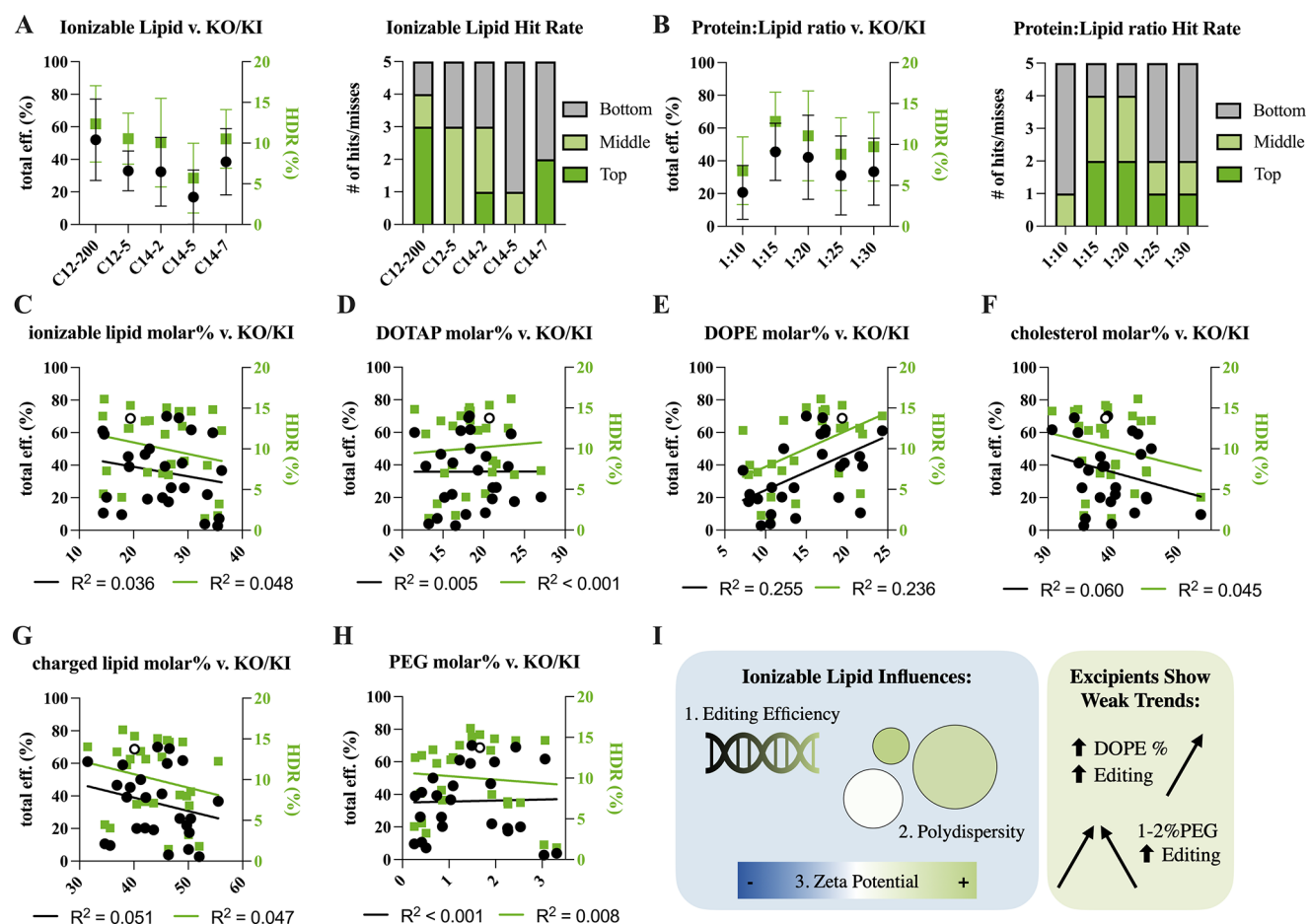


Figure 3. Identifying LNP components that significantly influence knockout and knock-in efficiencies. All excipients were modulated for this 25 LNP DOE screen: (A) ionizable lipid type, (B) the protein cargo-to-total lipid weight ratio, (C) ionizable lipid molar percent, (D) DOTAP molar percent, (E) DOPE molar percent, (F) cholesterol molar percent, (G) total charge lipid molar percent, both ionizable and DOTAP lipids, and (H) PEG-lipid molar percent. For each variable, the resulting molar percentages are plotted against gene editing efficiencies, both total efficiency and HDR. Based on multiple linear regression, all six variables tested influenced the resulting LNP. (I) However, only the ionizable lipid type and DOPE molar percent significantly influenced gene editing efficiency. Error bars show SD, and the hollow point represents the base LNP.

untreated cells. However, all delivery vehicles showed some reduction of PD-L1 signal, in a dose-responsive manner (Figure 2E), based on flow cytometry using anti-PD-L1 antibody staining. These same LNPs were evaluated for CD44 knockout in both HEPG2 and H1299 cells, and similar results were observed. Both the base and A14 LNPs were capable of reducing cell growth—as measured by CellTrace via flow cytometry—and A14 slightly outperformed the base LNP formulation (Figure S5).

A multiple linear regression was performed to explore which excipients had a significant impact on editing efficiency. For this analysis, all LNP characteristics measured, including excipient identity and ratio, as well as measured physicochemical characteristics, were included in the linear regression as independent variables. The resulting editing efficiencies were the dependent variable. From this analysis, it was found that the ionizable lipid identity was the strongest influence on efficiency (Figure 3A) and significantly impacted LNP polydispersity and zeta potential (Figures S4 and 3I). Protein-to-lipid ratio was also found to impact efficiency, with 1:15 and 1:20 weight ratios outperforming the other ratios tested. In contrast, many of the excipient ratios showed no or only weak trends (Figure 3C–H). However, there was

an increase in editing efficiency observed with increasing DOPE content (Figure 3E) and a goldilocks effect with 1–2% PEG content yielding the highest editing efficiency (Figure 3H).

High-Throughput DNA Barcoding to Evaluate In Vivo Biodistribution. While intracellular delivery and activity of the RNP complex and ssDNA are important metrics by which to evaluate these LNP formulations, it is equally important that the LNPs can deliver their cargo to organs and cell subtypes of interest in an *in vivo* setting. Further, it was hypothesized that top-performing LNPs in extrahepatic organs may be those that show only moderate transfection but improved tropism. To evaluate the importance of cellular delivery versus organ tropism, the same 25 LNP library was reformulated for *in vivo* screening, utilizing a high-throughput DNA barcoding approach.

For this study, a previously designed and validated library of DNA barcodes (b-DNA)⁴⁸ was introduced to the LNP formulations in place of the ssDNA donor. By including a unique b-DNA in each LNP formulation, all 25 LNPs could be pooled and injected as one for *in vivo* study (Figure 4A). By utilizing this molecular barcoding approach, we evaluated the biodistribution of these LNPs in a high-throughput manner—

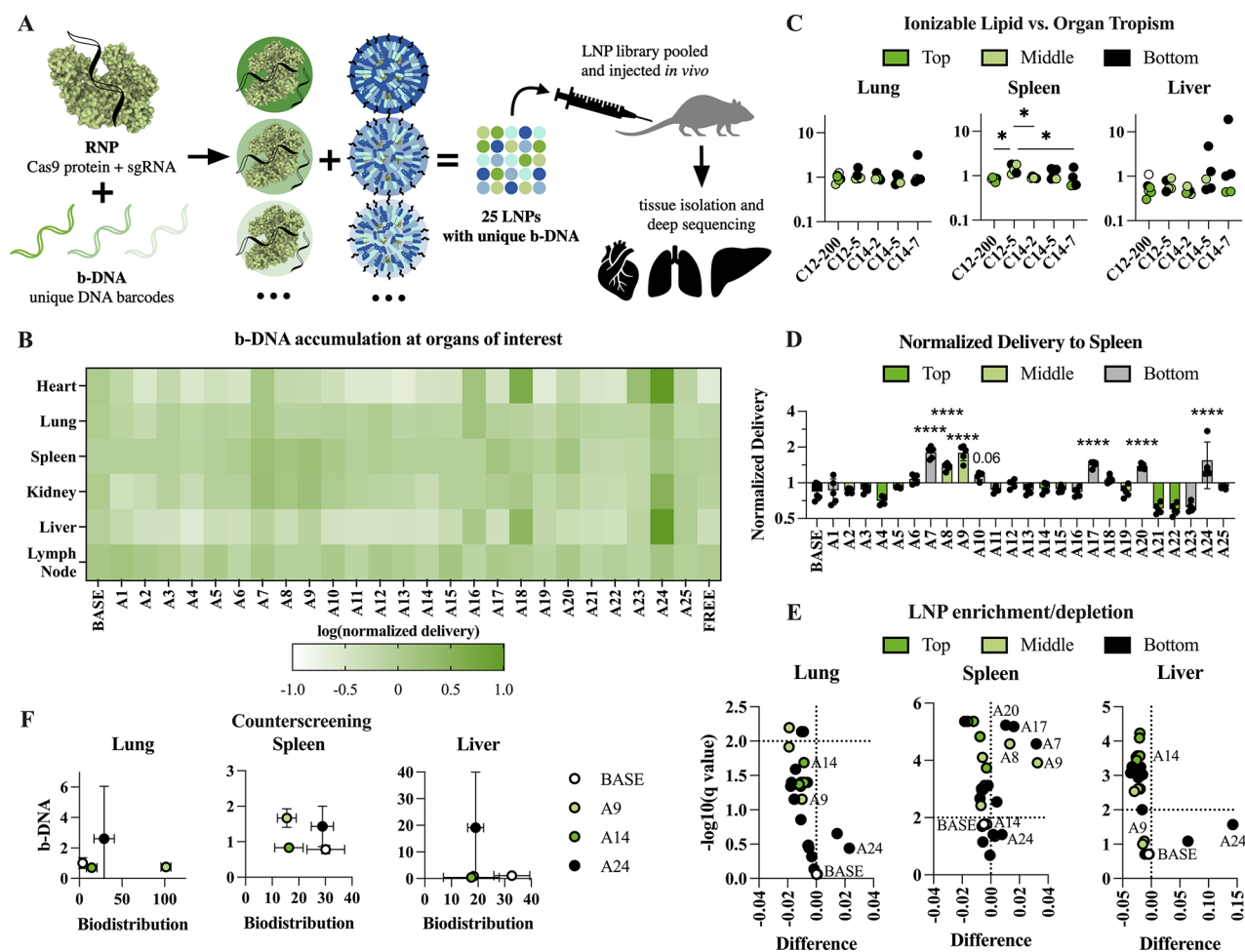


Figure 4. High-throughput evaluation of *in vivo* organ accumulation using DNA barcoding. (A) Aqueous phase of each LNP formulation contains RNPs and barcoded DNA (b-DNA). The same 25 LNP library is formulated—each LNP containing a unique DNA barcode—and pooled for *in vivo* administration. After administration, organs are harvested and processed for next-generation sequencing to count b-DNAs at each organ. (B) A heat map showing relative LNP accumulation at each organ. A24 was identified as a high accumulator in multiple organs. (C) Of all variables in the DOE library, only the ionizable lipid type was found to significantly influence organ tropism, with C12-5 resulting in significantly increased spleen accumulation. (D) Of all organs evaluated, the spleen was found to have the most variability between the base formulation and the other 25 LNPs tested. (E) Volcano plots of b-DNA accumulation in the lungs, spleen, and liver, showing LNP formulations with significantly enriched or depleted counts. Multiple LNP formulations were significantly enriched in the spleen. (F) Counter-screening results of four representative LNP formulations—the base LNP, A9, A14, and A24—showing a lack of agreement between individual and high-throughput accumulation, primarily due to differences in lung accumulation. $n = 5$ mice for b-DNA and $n = 3$ for counter-screening values are normalized to each experimental control; *: $p < 0.05$ and ****: $p < 0.0001$. Error bars show SD.

injecting the LNP pool to five mice—and further evaluating which LNP formulation parameters influence *in vivo* fate.

Six hours after IV administration, organs of interest—heart, lung, spleen, kidneys, liver, and lymph nodes—were harvested and processed for next-generation sequencing (NGS). Sequencing results were analyzed to obtain counts for each b-DNA in each tissue sample (Figure 4B). Due to the nature of the analysis, these counts can only be compared within each organ, not across the entire data set. As before, excipient content, ionizable lipid identity, and protein-to-lipid weight ratio were evaluated for their impact on b-DNA accumulation *in vivo*. From this analysis, the ionizable lipid type once again stood out as the only significant factor, with the C12-5 lipid specifically showing improved b-DNA accumulation in the spleen (Figure 4C). Interestingly, when compared against *in vitro* results, top-performing LNP formulations were found not to have enrichment in tissue b-DNA accumulation, with LNPs that were poor performers from the *in vitro* screen showing

higher accumulation in tissues of interest. Specifically, A7, A17, and A20—all poor performers *in vitro*—showed significant b-DNA enrichment in the spleen (Figure 4D,E). Similarly, while not significant, A18 and A24—also poor *in vitro* performers—showed increased counts in the liver (Figure 4E). While it is not studied further in this work, it is interesting to note the inverse relationship between *in vitro* efficiency and *in vivo* accumulation. It is possible that this is due to LNP stability and charge. Specifically, more stable particles may allow for increased circulation time *in vivo* but reduced endosomal escape. It is also noteworthy that the five LNP formulations mentioned—A7, A17, A18, A20, and A24—all have high surface zeta potentials, compared to the rest of the LNP library (Figure 4A).

Most interestingly, there were no significantly enriched b-DNAs in the lungs, with only A7 and A24 showing increased counts (Figure 4E). All LNPs within the library contain a positive charge, in the form of DOTAP, which has been

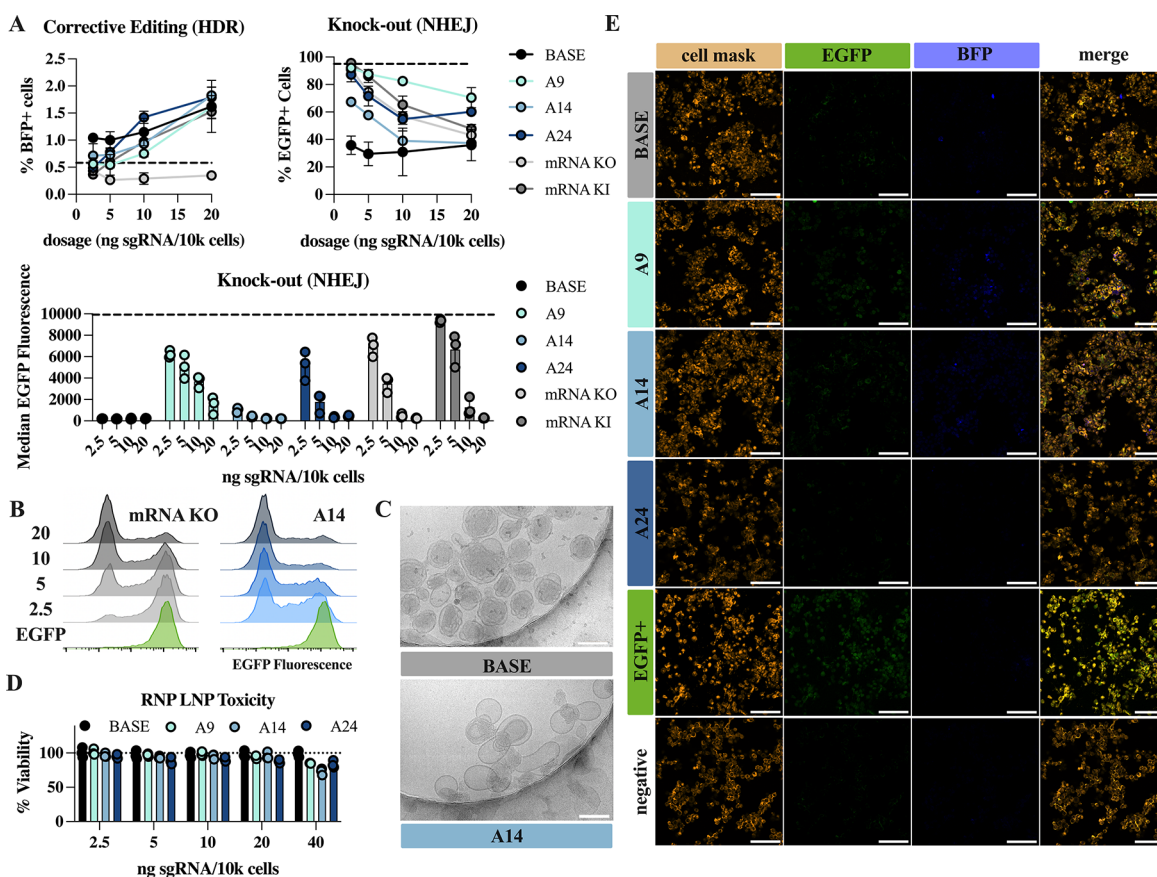


Figure 5. Four LNP formulations identified—the base LNP, A9, A14, and A24—show dose-responsive editing *in vitro* and limited toxicity only at the highest dose tested. (A) After 5 days, H1299 cells treated with RNP and ssDNA LNPs were analyzed via flow cytometry for BFP knock-in (KI) and EGFP knockout (KO). Dashed lines shown are untreated EGFP+ cell control. All KI LNPs were able to show BFP fluorescence, with the base and A14 formulations showing improved editing at lower dosages compared to other RNP LNPs and mRNA controls; $n = 3$. (B) Representative flow plots of mRNA KO and A14 LNPs show improved gene editing capabilities of the A14 LNP at lower dosages; $n = 3$. (C) Cryo-EM images of top editors—base and A14 LNPs—showing obvious differences in LNP physical structure, with A14 LNPs having larger surface lipid blebs, reducing overall sphericity. Scale bar = 100 nm. (D) A9, A14, and A24 show limited cell toxicity at 40 ng of sgRNA/10 000 cell dose; $n = 3$. (E) Representative confocal fluorescent images of H1299 cells 5 days after treatment with RNP and ssDNA LNPs at 20 ng of sgRNA/10k cells. There is a clear reduction in EGFP fluorescence in all RNP LNP groups, and BFP signal can be seen, especially in the base, A9, and A14 treated groups. Scale bar = 100 μm . Error bars show SD.

previously shown to influence LNP trafficking to the lungs. In previous protein delivery work, it has been shown that the lung tropic nature of DOTAP may be cargo-specific, with DOTAP-containing formulations still delivering small proteins primarily to the liver.^{42,45} However, it was still surprising to see no significant enrichment in the lung tissue samples.

With all high-throughput screens, it is important to carry out individual counter-screening to confirm results. For counter-screening, four LNPs were chosen to evaluate: (i) the base LNP, which exhibited high editing efficiency in the *in vitro* screen and has been reported in the literature to be primarily liver tropic, although it showed average accumulation (no enrichment or depletion) in the *in vivo* screen; (ii) A9, a middle performer in both *in vitro* and *in vivo* screens, with spleen enrichment and average editing efficiency; (iii) A14, which was the top performer from the *in vitro* screen but showed nonsignificant depletion in lung and liver b-DNA counts; and (iv) A24, the top performer from the *in vivo* screen, which showed nonsignificant enrichment but consistent accumulation across all organs of interest but low *in vitro* editing.

All four LNPs were dyed with DiR lipid dye and individually administered to mice intravenously at a dose of 0.1 mg/kg of sgRNA to evaluate biodistribution under individual conditions at therapeutically relevant dosages. Based on the b-DNA screen, it was expected that the A24 formulation would show the highest accumulation overall—in the lungs, liver, and spleen—and that A9 would show equal or higher spleen accumulation with slightly reduced liver and lung delivery. A14 was expected to show lower accumulation overall, and the base LNP formulation was expected to be average across all organs. In the counter-screen, the lung distribution was found to be highly variable among the four LNPs tested—with A9, A24, and A14 all showing higher lung accumulation than the base LNP—which did not align with the expected results based on the b-DNA data (Figure 4F).

It has been recently shown that the DOTAP-associated lung distribution observed in LNP formulations is tied to clotting, specifically to the thrombin-activated coagulation cascade and fibrinogen binding.⁴⁹ This effect was found consistently across multiple LNP formulations with various excipient contents—if the overall LNP zeta potential was significantly positive. While this mechanism can be harnessed to achieve extrahepatic

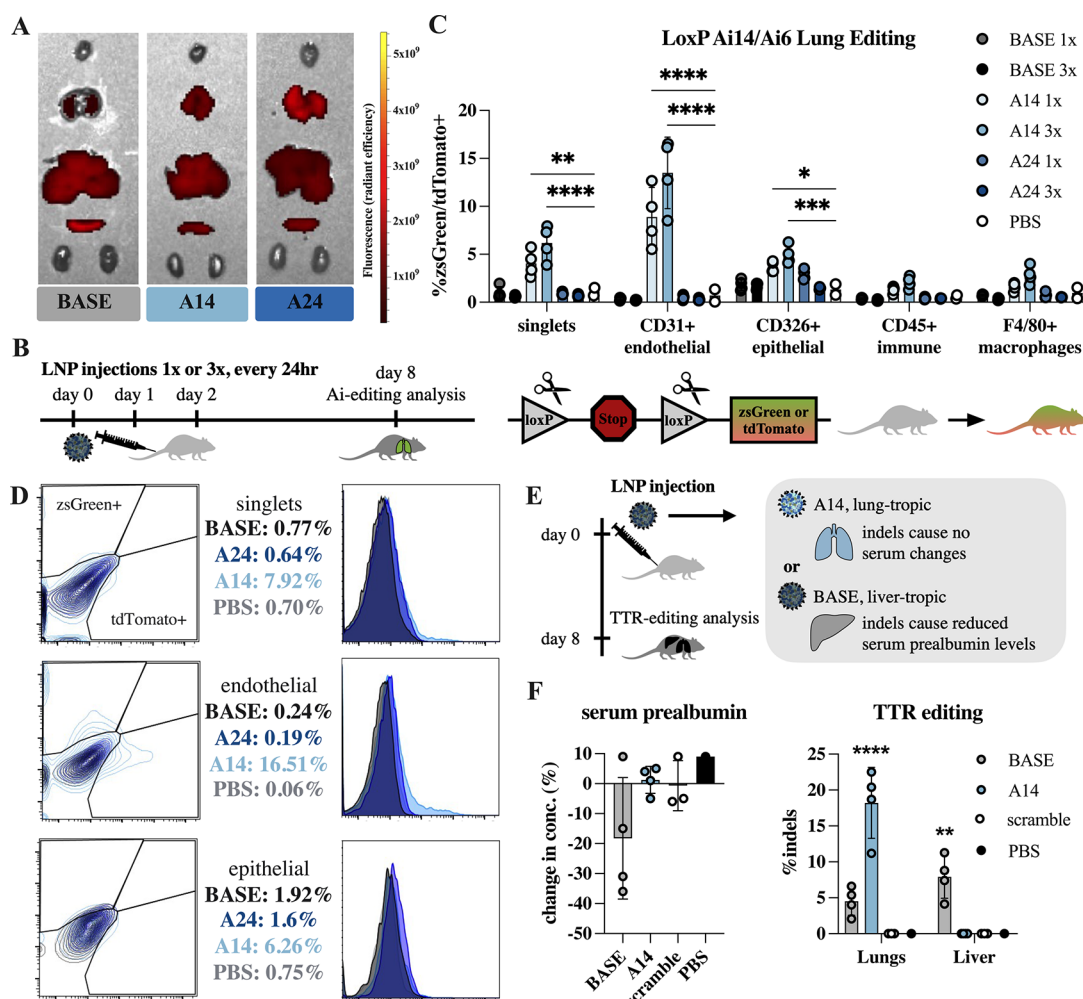


Figure 6. Base, A14, and A24 LNP formulations show variable biodistributions and gene editing *in vivo*. (A) Biodistribution data and representative IVIS images of DiR-dyed RNP and ssDNA LNPs. The base LNP shows primarily liver accumulation, while A14 and A24 have increasing levels of lung tropism. (B) Experimental scheme for *loxP/Ai* *in vivo* editing. LNPs are injected either once or three times via intravenous injection at a dose of 0.15 mg/kg sgRNA. Two sgRNAs—specific to upstream and downstream *loxP* sites—are used to cause excision of a stop cassette and expression of a reporter fluorophore. Ai14/Ai6 crosses are used to visualize single vs biallelic editing. (C) A14 shows dose-responsive editing in bulk lung singlets as well as endothelial and epithelial cells. The base formulation—which is an efficient editor but has limited lung delivery—and the A24 LNP—which has improved lung tropism but limited editing—show no significant increases in fluorescence. $n = 4$. (D) Representative flow plots showing the gating scheme and editing efficiencies for singlet, endothelial, and epithelial populations. (E) Experimental scheme for TTR editing, a clinically relevant gene editing target. (F) TTR serum levels—measured via ELISA—and organ indels—measured by NGS sequencing—of base LNP, A14, and controls. The base LNP shows editing in both the lungs and the liver, causing a reduction of serum levels, while the A14 LNP shows editing only in the lungs, with no liver indels or serum reduction, indicating true extrahepatic delivery efficiency; $n = 4$. *: $p < 0.05$, **: $p < 0.01$, ***: $p < 0.001$, and ****: $p < 0.0001$. Error bars show SD.

delivery, it often comes with severe toxicity risk, especially in cases with larger LNPs, preexisting inflammation, or higher LNP dosages. Based on these findings, it is our hypothesis that the lung-tropic nature of DOTAP-containing LNPs is not accurately reflected within high-throughput *in vivo* methods such as DNA barcoding. We believe this is due to two factors: (i) the dose-sensitive function of this mechanism may be such that the relatively small dose of an individual LNP (77 ng ssDNA/LNP formulation/mouse) may not be high enough to activate coagulation and clotting on the scale necessary to observe lung filtration and tropism and (ii) if coagulation is activated within a mouse, the resulting clotting may equally or significantly affect all LNPs in the pool, not just the single or few LNPs that triggered thrombin binding and the resulting cascade. Between these two factors and based on these

experimental results, it is our belief that DOTAP-associated lung distribution cannot be accurately measured from high-throughput screens without further optimization of or changes to the b-DNA experimental setup.

If accumulation within the counter-screen is evaluated with the assumption that lung accumulation within the *in vivo* screen is inaccurate, then the results of the counter-screen align more closely with what is expected. A9—with the highest lung accumulation in the counterscreen—shows comparative reduction in liver and spleen accumulation, which still remains lower than the base LNP. Similarly, A24 and A14—with lesser but still increased lung accumulation—show lesser comparative reduction in the liver and spleen, with A24 still outperforming A9 and A14 in liver and spleen accumulation, as expected. Finally, the base LNP formulation—with the

lowest lung accumulation—has the least reduction in the liver and spleen and the most liver accumulation overall, which was expected based on previous studies in the literature (Figure 4F).

Identified Formulations Show Corrective Editing *In Vitro*. While the counter-screening results did not entirely align with the high-throughput screen, the four identified LNP formulations—the base LNP, A9, A14, and A24—remained an interesting spread of *in vitro* activity and *in vivo* distribution. Specifically, the base LNP was identified as a strong editor with primarily liver delivery; A14 and A24 were identified as having improved lung tropism but strong and weak editing activity, respectively, and A9 was identified as having the best lung delivery, with only mediocre editing efficiency. Therefore, the same four LNPs were moved forward to additional *in vitro* testing to identify any additional differences between these formulations. Previously published Cas9 mRNA LNP formulations—both knockout (KO) and knock-in (KI)—were included to compare LNP RNP delivery to more traditional mRNA cargo.

All four RNP LNP formulations, as well as the KI mRNA LNP, were able to show corrective editing of EGFP to BFP in a dose-responsive manner (Figure 5A), as measured by BFP fluorescence via flow cytometry. Looking specifically at EGFP fluorescence, the top *in vitro* editors—the base LNP and A14—outperform all other formulations tested at low dosages. A9 and A24, as less efficient editors, perform more similarly to the mRNA controls. As before, all LNPs can reduce EGFP similarly at higher dosages (Figure 5A,B). Although the base LNP and A14 formulations performed very similarly *in vitro*, they exhibited drastically different shapes and structures, as visualized by cryo-EM (Figure 5C). Specifically, the base formulation shows a tightly packed core with thinner outer lipid layers in a petal-like shape, and the LNPs are generally spherical. In contrast, the A14 formulation has much larger outer lipid layers, which form irregular blebs, causing the LNP to take on a less spherical shape overall. All four RNP LNPs also showed similar toxicities *in vitro*, with a slight reduction in cellular viability at the highest dosage tested—40 ng sgRNA/10k cells—in the A9, A14, and A24 formulations (Figure 5D). Finally, the EGFP-to-BFP edit was further confirmed in all RNP LNP formulations via confocal microscopy and cellular staining, where all formulations showed a clear reduction in EGFP signal at the 20 ng sgRNA/10k cell dose, and clear BFP signal can be seen in the base, A9, and A14 formulations (Figure 5E).

A Lung-Specific LNP Formulation for Editing in Epithelial Cells, Endothelial Cells, and of Clinical Targets. As mentioned previously, strong lung tropism caused by DOTAP can cause significant toxicity due to clotting in the lungs. Due to this, the A9 formulation—which was the strongest lung tropic lipid (Figure 6A) but also had the highest molar percentage of charged lipid (both ionizable and DOTAP) of all LNPs tested—was excluded from additional *in vivo* testing, as acute toxicities were observed. Interestingly, the A14 and A24 formulations—which contain higher molar percentages of DOTAP—did not seem to result in similar levels of toxicity, possibly due to their lower total charged lipid contents. Nevertheless, only A14 and A24 were moved forward to continual *in vivo* testing as similarly improved lung delivery vehicles with variable *in vitro* editing efficiencies.

To evaluate editing efficiency *in vivo*, Ai14/Ai6-crossed mice were dosed with RNP LNPs—base, A14, and A24—which

contained two sgRNAs. Each sgRNA is specific for either the upstream or the downstream loxP site within the Ai cassette (Figure 6B). Through successful cutting at both loxP sites, the stop cassette will be removed, causing strong expression of either zsGreen or tdTomato fluorescence. As these mice have one allele of each reporter fluorophore color, Ai14/Ai6 crosses are used to visualize single vs biallelic editing. Of note, very few cells were found to have evidence of biallelic editing, with most edited cells expressing only tdTomato or zsGreen (Figure S8). Through this model, the LNP editing efficiency can be evaluated in organs and cell subtypes of interest.

After either one or three IV LNP injections, the lungs were harvested and processed for flow cytometry. CD31+ endothelial cells, CD326+ epithelial cells, CD45+ immune cells, and F4/80+ macrophages were specifically evaluated for loxP editing. Of all three LNPs tested, only A14 showed significant editing in the lung. Editing was observed in both the bulk lung singlets as well as the endothelial and epithelial populations, and editing in all populations was dose-responsive (Figure 6C), reaching efficiencies of nearly 8% in singlets, 16% in endothelial cells, and 6% in epithelial cells (Figure 6D).

While these numbers may seem low, it is important to note that this assay, while sensitive in terms of fluorescence due to the strong promoter downstream of the fluorophore, requires the dual cutting of two separate sgRNA sites. It has been shown that editing with these loxP guides is highly dependent on the kinetics and timing of these two double-stranded breaks, and that indel formation is often much higher at each cut site than overall fluorescence.⁵⁰ This is, in part, because indels can cause the loss of the sgRNA recognition site sequence, causing repeat dosages to only minimally impact efficacy, as there are fewer available sites to cut.

To test this editing in a clinically relevant target—as opposed to a reporter model—the A14 and base formulations were additionally tested in a transthyretin (TTR) editing model. Transthyretin amyloidosis is caused by genetic mutations that result in misfolded TTR—also known as prealbumin—which in turn causes the formation and buildup of amyloid fibrils in the heart and peripheral nerves.⁵¹ By knocking down the production of these misfolded TTR proteins in the liver, we can reduce amyloid deposits in tissues. Because of this, CRISPR-Cas9 editing for this application has recently entered clinical trials.⁵² In this model, successful knockout of the target in the liver should cause a reduction in serum levels of TTR. Editing of the TTR locus in other organs, such as the lungs, should not result in changes to serum levels, regardless of indel percentages (Figure 6E).

When formulated with TTR-targeted sgRNA, both the base and A14 LNP formulations resulted in *in vivo* gene editing and indel formation (Figure 6F). The base LNP shows approximately 5% indels in the lungs and almost 10% indels in the liver, resulting in a nonsignificant but noticeable reduction in serum prealbumin, as measured by ELISA. In contrast, A14 shows no liver indel formation, and all editing is localized to the lungs, with nearly 20% indel formation and no reduction in serum levels (Figure 6F). This shows that the A14 formulation can efficiently edit native genes as well as reporter loci with no apparent off-target liver editing. The mechanism causing no editing in the liver—even when LNP fluorescence can be seen in biodistribution studies—is currently unknown. There are two major categories of likely mechanisms: (1) reduced cellular uptake in the liver, indicated by tissue accumulation but no cellular entry, or (2) reduced endosomal

escape and nuclear localization. There are multiple significant differences between the base LNP and the A14 formulation, which may contribute to this effect and could have impact on either category. A14 has a higher apparent zeta potential and a larger and less spherical size than the base LNP (Figures 3 and 5C), which likely influences protein corona content. This, in turn, may influence cellular uptake—for example, through activation of different endocytic mechanisms. As different cell types have been shown to have different endolysosomal properties,⁵³ these seemingly minor characteristic changes may result in very different fates for LNPs in liver vs lung cell types. This, along with the innate characteristics of the LNP—in both its original form and any lipid structures that remain after endosomal uptake/escape—may influence cellular processes such as endosomal recycling and nuclear transport. Ultimately, while the mechanism for the extrahepatic nature of A14's editing efficiency is currently unknown, this formulation remains a highly effective lung-editing LNP that demonstrates no off-target editing in the liver.

CONCLUSIONS

In this work, we aimed to utilize both *in vitro* and high-throughput *in vivo* screening methodologies to identify LNP formulations and parameters that can intracellularly deliver CRISPR-Cas9 RNPs—with or without ssDNA—to extrahepatic tissues and cell types, specifically, within the lungs. Ultimately, it was found that, while highly efficient in some circumstances, high-throughput b-DNA screening was inaccurate when DOTAP-associated mechanisms for lung delivery are involved in LNP tropism. Therefore, while the utilization of b-DNA in place of ssDNA may be effective for other screens, the utilization of it for systemic IV delivery of RNPs cannot be recommended without further optimization or changes to the overall b-DNA setup.

Regardless, a highly effective lung-editing LNP was identified, A14, which appears to be truly extrahepatic, with no liver editing observed in the clinically relevant TTR editing model. Further, this LNP is able to edit both endothelial and epithelial cells within the lung, creating up to 20% indels after a single dosage. It is difficult to assess what level of gene editing in the lung will be needed to observe phenotypic changes and improvements in patient lives. In the case of Cystic Fibrosis, *in vitro* models estimate that editing in 25% of surface epithelial cells would restore normal mucus transport and that even lower percentages could be effective in more specialized cell types.⁵⁴ Others have shown that even low editing efficiencies—around 1–2%—can restore a meaningful amount of function (~30% of WT).⁵⁵ In other tissues, such as the liver, gene editing has been shown to have therapeutic effect and improve outcomes with as little as 10% editing efficiency.⁵⁶ For each genetic disease, success will look different, but there is evidence that the efficiencies seen in this work may be enough to have a significant impact for some patient populations.

METHODS/EXPERIMENTAL

Ionizable Lipid Synthesis and LNP Formulation. The ionizable lipids used in this study (Table S2) were synthesized by reacting epoxide-terminated alkyl chains (Avanti Polar Lipids; Alabaster, AL) with polyamine cores (Enamine; Monmouth Jct, NJ) using S_N2 addition reactions, as previously described.^{43,57} Components were combined with 7 equivalents of alkyl epoxides and mixed with a magnetic stir bar for 48 h at 80 °C. The crude product was then transferred to a Rotavapor R-300 (BUCHI; Newark,

DE) for solvent evaporation. For initial screening, the lipids were suspended in ethanol for use in the formulation without further purification. Identified top lipids were purified using a CombiFlash (Teledyne; Thousand Oaks, CA) for further *in vitro* and *in vivo* testing, and structures were confirmed using LC-MS. Nominal mass accuracy LC-MS data were obtained using a Waters (Milford, MA, USA) Acquity UPLC system equipped with a Waters TUV detector (254 nm) and a Waters SQD single quadrupole mass analyzer with electrospray ionization. Samples were prepared in 200-proof ethanol and injected onto an Acquity UPLC BEH C8 1.7 μm , 2.1 mm \times 50 mm column with a 2-min wash followed by a gradient mobile phase from 50% water (1% trifluoroacetic acid) and 50% acetonitrile (1% trifluoroacetic acid) to 100% acetonitrile (1% trifluoroacetic acid) over 8 min.

Lipid nanoparticles (LNPs) were formulated by mixing an ethanol phase and an aqueous phase in a staggered herringbone microfluidic device (produced in-house) in a 1:3 volume ratio using pump33DS syringe pumps (Harvard Apparatus; Holliston, MA), as previously described.^{36,43} The ethanol phase contained ionizable lipid, 1,2-dioleoyl-*sn*-glycero-3-phosphoethanolamine (DOPE, cat. no. 850725, Avanti Polar Lipids; Alabaster, AL), 1,2-dioleoyl-3-trimethylammonium-propane (DOTAP, cat. no. 890890, Avanti Polar Lipids), cholesterol (cat. no. 57-88-5, ThermoFisher), and 1,2-dimyristoyl-*sn*-glycero-3-phosphoethanolamine-*N*-[methoxy(polyethylene glycol)-2000] (PEG, cat. no. 880150, Avanti Polar Lipids).

The aqueous phase contained a solution of 1 \times phosphate-buffered saline (PBS), the ribonucleoprotein (RNP) cargo, and ssDNA in the case of knock-in experiments. RNPs were formed by adding TrueCut Cas9 protein (Thermo Fisher Scientific; Waltham, MA) and single guide RNA (sgRNA) modified with 2'-O-methyl at the 3 first and last bases and 3' phosphorothioate bonds between the first 3 and last 2 bases (standard modifications supplied by Synthego; Redwood City, CA). Cas9 and sgRNA were added in a 1:1 molar ratio and allowed to sit at room temperature for 20 min—allowing time for RNP complexes to form—before microfluidic mixing of the two phases. In the case of knock-in experiments, ssDNA was added at equal molar ratio to the Cas9 and sgRNA. After synthesis, LNPs were subsequently dialyzed against 1 \times PBS in 20 kDa molecular weight cutoff dialysis cassettes for 1 h to remove ethanol.

RNP Lipid Nanoparticle Characterization. To evaluate size, 10 μL of LNPs were diluted 100 \times in 1 \times PBS in disposable cuvettes for dynamic light scattering (DLS) measurements on the Zetasizer Nano (Malvern Instruments; Malvern, UK). LNP size (Z-average diameter) and polydispersity index (PDI) are reported as the mean \pm standard deviation ($n = 3$ measurements). To quantify surface zeta potential, 10 μL of LNPs were diluted 100 \times in water (pH 7) and measured in DTA1070 zeta potential cuvettes (Malvern Panalytical, Malvern, UK) on the Zetasizer Nano.

To determine Cas9 protein concentration, LNP samples were measured using a micro-BCA protein assay as per the manufacturer's instructions (Thermo Fisher Scientific; Waltham, MA). LNPs were diluted in PBS with 2% SDS to accommodate the presence of lipids in the sample. BCA working reagent was added to each sample, and the samples were incubated for 2 h at 37 °C. Samples were added in triplicate to 96-well plates, and the resulting absorbance was measured on a plate reader alongside a standard curve to quantify protein concentration. Concentration values are reported as the mean \pm standard deviation ($n = 3$ measurements).

To determine the sgRNA concentration, LNP samples were measured using a RiboGreen assay as per the manufacturer's instructions (Thermo Fisher Scientific). LNP samples were diluted in either TE buffer (to measure free or surface-anchored RNA only) or TE buffer with 0.1% Triton-X (to allow for quantification of total RNA). Proteinase K and DNase were added to all samples. Samples were added in triplicate to 96-well plates, and the resulting fluorescence was measured on a plate reader alongside a standard curve to quantify RNA concentration and encapsulation (total RNA versus free RNA). To determine the ssDNA concentration, a similar protocol was followed with an OliGreen assay (Thermo Fisher

Table 1. PCR Primers and sgRNAs

Gene	F primer (5' to 3')	R primer (5' to 3')	sgRNA
EGFP	ATGGTGAGCAAGGGCGAG	TTACTTGTACAGCTCGTCCATG	GCUGAAGCACUGCACGCCGU
CD44	CCCAGTTCATGCCATTCT	GAAAGGAGCCTTCCAGTTCTAA	GAAUACACCUGCCAAAGCGGC
PD-L1	GCTCTTTCCTGAACTCCATACC	GTCTTCCTCTCCATGCACAAA	GGUUCCEAAGGACCUAUAUG

Scientific), with the addition of RNase instead of DNase to each sample.

Cell Culture and In Vitro Delivery Assays. GFP+ H1299s were gifted by Mohamad-Gabriel Alameh. Negative H1299s were purchased from ATCC and transfected to express BFP using lentiviral vectors purchased from Tailored Genes Inc. (Toronto, ON). To generate BFP, the cells were incubated overnight with different volumes of lentivirus in complete RPMI medium supplemented with 8 $\mu\text{g}/\text{mL}$ Polybrene. The following day, the medium was replaced, and the cells were grown to confluence. Cells expressing BFP were isolated using FACS. These cell lines were maintained in complete RPMI media containing 10% FBS and 1% penicillin/streptomycin.

In a typical delivery assay, 10,000 cells were seeded in a 96-well plate format. For CRISPRmax (Invitrogen; Waltham, MA) delivery, 0.5 μL of Cas9 Reagent was added to 1 μL of Cas9 protein (50 $\mu\text{g}/\text{mL}$) and 0.2 μL of sgRNA (50 $\mu\text{g}/\text{mL}$) in 5 μL of media. This was then mixed with 0.3 μL of CRISPR Reagent in 5 μL of media and incubated for 10 min at room temperature to promote complexation before adding to cells. For LNP delivery, the indicated amounts were added directly to each well. Twenty-four hours after dosing, LNPs or CRISPRmax was removed and media was replaced. For genomic DNA (gDNA) extraction, which was used for sequencing, a Monarch Genomic DNA Purification Kit (New England Biolabs; Ipswich, MA) was used according to manufacturer's protocols 48 h after treatment. For longer-term studies, 48- or 24-well plates were used, and an additional media change occurred every 48 h, but cells were still seeded at 10,000 on day 0.

For flow cytometry, analysis occurred 3–5 days after treatment depending on the readout. At the end point, cells were detached with trypsin and pelleted in a 4 $^{\circ}\text{C}$ table-top centrifuge at 600 g . Cell pellets were washed once with PBS and resuspended in a flow buffer (PBS, 1% w/v BSA, 1 mM EDTA). SYTOX red was added according to manufacturer's instructions, and samples were analyzed on a BD LSR II flow cytometer (BD Biosciences; Franklin Lakes, NJ). At least 10,000 total events were collected. Data analysis was carried out using FlowJo v10. The gate for fluorophore positivity is defined based on the negative cell control, and the positive gate is defined such that only 1% of the negative control sample would fall within that positive gate. Representative flow plots were generated in FlowJo v10. Data reported are of live cells only, as determined based on SYTOX staining, and are reported as the mean \pm standard deviation ($n \geq 3$ measurements). Median fluorescence expression is reported instead of the percentage of the population in cases where there is not a clear positive population (e.g., a shift in the population in the positive control as opposed to a clear positive and negative population) to reduce errors based on gating.

To evaluate *in vitro* toxicity, cells were seeded in 96-well plates at 10,000 cells in 100 μL of media. Then, 24 h after seeding, LNPs were added. Cells were incubated with LNPs for 24 h, after which 100 μL of CellTiter-Glo (Promega) was added to each well, as per the manufacturer's instructions. Following incubation for 10 min, luminescence was measured using a plate reader. Luminescence was normalized within each plate to untreated cells and reported as the mean \pm standard deviation ($n \geq 3$ measurements).

Sanger Sequencing. PCR was performed to amplify gDNA regions of interest using Q5Master Mix (New England Biolabs), as per the manufacturer's instructions, with 10 μM of both forward and reverse primers. Primers for each region of interest are listed in Table 1.

The PCR product was run through gel electrophoresis using 1% E-Gel Agarose Gels (Invitrogen) run on an E-Gel Power Snap Electrophoresis System (Invitrogen). DNA bands were excised and

purified using Monarch DNA Gel Extraction Kit (New England Biolabs), as per manufacturer's protocol. Purified PCR product was quantified using absorbance on a plate reader with the NanoQuant plant (Tecan). To sequence regions of interest, the purified PCR product was diluted with water and 1 μM primer and submitted for Sanger sequencing by the DNA sequencing Lab at the Penn Genomic and Sequencing Core. The resulting sequencing files were visualized using SnapGene and analyzed using TIDER.^{58,59}

In Vivo DNA Barcoding. The b-DNAs used in this study are 61bp ssDNAs. The barcode region is composed of 10 nucleotides in the center of the oligonucleotide, with an additional 10 random nucleotides included at the 3' end of the barcode region. The inclusion of unique molecular identifiers (UMIs) provides error correction and increased accuracy during sequencing. The 5'- and 3'-ends of each b-DNA are conserved and contain priming sites for Illumina adapters. These b-DNA sequences have been previously published⁴⁸ and were synthesized and purified by Integrated DNA Technologies.

To evaluate LNP biodistribution, LNPs were formulated with unique b-DNAs and then pooled—along with a nonencapsulated b-DNA—for IV administration to female C57BL/6 mice. Next, 77 ng of each b-DNA was administered per mouse for a total dosage of 0.1 mg/kg sgRNA. Six hours post-LNP administration, mice were sacrificed and organs of interest were harvested, snap-frozen in liquid nitrogen, and powdered using a Geno/Grinder (SPEX Sample Prep). The resulting sample was stored in a -80°C freezer until analyzed.

To extract DNA from the tissue samples, tissue lysis buffer and a Zymo DNA purification kit (Zymo Research) were used as per the manufacturer's instructions. PCR was performed to amplify b-DNAs using Q5Master Mix (New England Biolabs), as previously described.⁴⁸

PCR products were run through gel electrophoresis and purified as described above. The purified PCR product was kept at -20°C . Next-generation deep sequencing was performed using Illumina MiSeq (Illumina). PCR product pools were quantitated using Qubit (Invitrogen) and pooled for equal DNA from each organ. This pool was submitted for sequencing to the Penn Next-Generation Sequencing Core (NGSC).

Resulting FASTQ files were analyzed using code that is available upon request. In brief, the Python tool `umi_tools` was used to count each LNP barcode within each organ barcode sample. b-DNA counts were normalized to the uninjected pool, and delivery to a specific organ was determined using the total sequencing reads in that tissue, as previously described.⁴⁸

Confocal Microscopy. Cells were seeded at 40,000 cells in 400 μL media in cell culture chamber slides. Twenty-four hours later, LNPs were added at 20 ng sgRNA/10k cells, and 24 h after treatment, the media was replaced. Seventy-two hours after treatment, cells were stained with SYTO red nuclear stain (ThermoFisher) and CellMask orange (Invitrogen). After staining, cells were fixed using 4% PFA, and coverslips were mounted. Samples were kept at 4 $^{\circ}\text{C}$ until imaging. Cells were imaged on a Zeiss LSM 710 Confocal microscope, maintained by the Perelman School of Medicine's Cell & Developmental Biology (CDB) Microscopy Core.

In Vivo LNP Fluorescence Biodistribution. For counter-screening, LNPs were concentrated using Amicon Ultra centrifugal filters (100 kDa MWCO, Millipore Sigma) and labeled with DiR (Thermo Fisher Scientific; Waltham, MA), a lipophilic carbocyanine that is weakly fluorescent in water but highly fluorescent and photostable when incorporated into membranes. Mice (C57BL/6J) were treated with 0.1 mg/kg of sgRNA via intravenous (IV) injection of the lateral tail vein. After 6 h, mice were sacrificed, and organs were

excised and imaged using the *in vivo* imaging system (IVIS) Spectrum (PerkinElmer; Waltham, MA). Fluorescence values are normalized to background fluorescence values for each organ, measured from a negative (PBS injection) mouse and reported as the mean \pm standard deviation ($n = 3$ measurements).

LoxP In Vivo Editing. Ai14/Ai6 crosses were generated as previously described.⁵⁰ In brief, Ai6 (B6.Cg-Gt(ROSA)-26Sor^{tm6(CAG-zsGreen1)Hze/J}, Stock No: #007906) and Ai14 (B6.Cg-Gt(ROSA)26Sor^{tm14(CAG-tdTomato)Hze/J}, Stock No: #007914) were obtained from Jackson Laboratories. Ai14 and Ai6 mice were crossed to generate compound heterozygous Ai14/Ai6 mice, with each containing one copy of a tdTomato (Ai14) floxed allele and one copy of a zsGreen (Ai6) floxed allele. Offspring from these crosses were confirmed for genotype using PCR primers and protocols available on the Jackson Laboratory website.

Ai14/Ai6 crosses were injected intravenously (IV) with 0.15 mg sgRNA/kg of RNP-encapsulating LNPs daily for 3 days. RNP LNPs contained two sgRNAs (Synthego) in equal parts with the following target sequences:

- upstream LoxP: 5'-AAAGAAUUGAUUUGAUACCG-3'
- downstream LoxP: 5'-GUAUGCUAUACGAAGUUAUU-3'

Seven days after the last injection, mice were sacrificed, and organs were harvested for IVIS imaging, flow cytometry, and histology. Sections of the lungs, livers, and spleens were collected for histology processing, and the remaining tissue was processed for flow cytometry. Lungs and livers were minced using a sterile blade and transferred to digestion medium containing DNase (New England Biolabs; Ipswich, MA), collagenase II and IV, and in the case of livers, Dispase II (Fisher Scientific; Hampton, NH), for 1 h at 37 °C. Spleens were smashed against a cell strainer and moved directly to centrifugation and washing steps. All organs were treated with ACK Lysis Buffer and ultimately processed to a single-cell suspension in 1 \times PBS + 0.1% BSA + 2 mM EDTA.

Lungs and livers were stained for CD31, CD326, CD45, and F4-80 expression (BioLegend; San Diego, CA, and Fisher Scientific) to isolate endothelial cells, epithelial cells, immune cells, and macrophages/Kupffer cells, respectively. Spleens were stained for CD3, CD19, and F4-80 expression (BioLegend) to isolate T cells, B cells, and macrophages, respectively. tdTomato positivity was used to identify cells with successful LoxP stop cassette editing in the Ai9 cassette in the bulk organs (singlets), as well as the identified cell type populations.

TTR In Vivo Editing. Mice (C57BL/6J) were injected intravenously (IV) with 0.15 mg of sgRNA/kg of RNP-encapsulating LNPs. RNP LNPs contained sgRNA (Synthego) targeting TTR: 5'-UUACAGCCACGUCUACAGCA-3'. One week after IV administration of LNPs, the mice were sacrificed, and their lungs were harvested. The lungs were minced using a sterile blade, and gDNA was extracted using a Monarch Genomic DNA Purification Kit (New England Biolabs). PCR amplification of the target amplicon was carried out as described above using the following primer sequences:

- mTTR-exon2-F, 5'-CGGTTTACTCTGACCCATTTTC-3'
- mTTR-exon2-R, 5'-GGGCTTCTACAAGCTTACC-3'

Full-length Illumina sequencing adapters were added to PCR products using a Nextera XT DNA Library Preparation Kit (Illumina, San Diego, CA). Pooled samples were sequenced using an Illumina MiSeq system. Alignment of fastq files to the target amplicon and quantification of editing frequency at the TTR locus were performed using CRISPResso2.⁶⁰

Statistical Analysis. Statistical analyses—including multiple and simple linear regression analyses—were performed on GraphPad Prism (v10) software. If it is otherwise unspecified, ANOVA was applied as appropriate. Statistical significance was defined at $\alpha = 0.05$. Multiple batches of LNP, Cas9 protein, and sgRNAs were used throughout this study.

ASSOCIATED CONTENT

Supporting Information

The Supporting Information is available free of charge at <https://pubs.acs.org/doi/10.1021/acsnano.4c16617>.

Characterization of LNPs used throughout this work, DOE design table, preliminary buffer screening, additional correlation analyses, additional *in vitro* data, representative flow gating scheme, additional *in vivo* data, chemical structures of ionizable lipids used in this work (PDF)

AUTHOR INFORMATION

Corresponding Author

Michael J. Mitchell – Department of Bioengineering, University of Pennsylvania, Philadelphia, Pennsylvania 19104, United States; Penn Institute for RNA Innovation, Perelman School of Medicine, University of Pennsylvania, Philadelphia, Pennsylvania 19104, United States; orcid.org/0000-0002-3628-2244; Email: mjmitch@seas.upenn.edu

Authors

Rebecca M. Haley – Department of Bioengineering, University of Pennsylvania, Philadelphia, Pennsylvania 19104, United States; orcid.org/0000-0001-7322-7829

Marshall S. Padilla – Department of Bioengineering, University of Pennsylvania, Philadelphia, Pennsylvania 19104, United States; orcid.org/0000-0003-3607-790X

Rakan D. El-Mayta – Department of Bioengineering, University of Pennsylvania, Philadelphia, Pennsylvania 19104, United States

Ryann A. Joseph – Department of Bioengineering, University of Pennsylvania, Philadelphia, Pennsylvania 19104, United States; orcid.org/0000-0002-0795-6094

Jesse A. Weber – Raymond G. Perelman Center for Cellular and Molecular Therapeutics, The Children's Hospital of Philadelphia, Philadelphia, Pennsylvania 19104, United States; Cell and Molecular Biology Graduate Group, Perelman School of Medicine, University of Pennsylvania, Philadelphia, Pennsylvania 19104, United States

Christian G. Figueroa-Espada – Department of Bioengineering, University of Pennsylvania, Philadelphia, Pennsylvania 19104, United States; orcid.org/0000-0003-2700-7678

Alvin J. Mukalel – Department of Bioengineering, University of Pennsylvania, Philadelphia, Pennsylvania 19104, United States

Adele S. Ricciardi – Department of Bioengineering, University of Pennsylvania, Philadelphia, Pennsylvania 19104, United States

Rohan Palanki – Department of Bioengineering, University of Pennsylvania, Philadelphia, Pennsylvania 19104, United States; orcid.org/0000-0001-5168-5634

Hannah C. Geisler – Department of Bioengineering, University of Pennsylvania, Philadelphia, Pennsylvania 19104, United States

Matthew T. Jester – Department of Bioengineering, University of Pennsylvania, Philadelphia, Pennsylvania 19104, United States

Beverly L. Davidson – Raymond G. Perelman Center for Cellular and Molecular Therapeutics, The Children's Hospital of Philadelphia, Philadelphia, Pennsylvania 19104,

United States; Department of Pathology and Laboratory Medicine, University of Pennsylvania, Philadelphia, Pennsylvania 19104, United States

Complete contact information is available at:
<https://pubs.acs.org/10.1021/acsnano.4c16617>

Author Contributions

R.M.H. was responsible for the conceptualization and writing of the manuscript. M.S.P., R.E., and J.A.W. assisted R.M.H. with experimental design. R.M.H., M.S.P., R.E., R.A.J., J.A.W., C.G.F.-E., A.J.M., A.S.R., R.P., H.C.G., and M.T.J. carried out experiments and collected data. J.A.W., C.G.F.-E., and A.J.M. assisted R.M.H. with data analysis. B.L.D. provided resources instrumental to this work, and M.J.M. was responsible for administration and funding. All authors read and reviewed the final manuscript.

Notes

The authors declare the following competing financial interest(s): RMH and MJM have filed a patent application on the lipid nanoparticle technology described in this manuscript. The other authors declare no competing interests.

ACKNOWLEDGMENTS

R.M.H., C.G.F.-E., A.J.M., and H.C.G. were supported by the National Science Foundation Graduate Research Fellowship Program (NSF-GRFP) under Grant No. DGE-2236662. M.S.P. was supported by the National Institute of Dental & Craniofacial Research (NIDCR) of the National Institutes of Health (NIH) under Award Number T90DE030854 and the Center for Innovation & Precision Dentistry (CiPD) at the University of Pennsylvania. R.A.J. was supported by a Jumpstart for Juniors grant from the Center for Undergraduate Research and Fellowships (CURF) and an Undergraduate Research Grant from Advancing Women in Engineering (AWE). C.G.F.-E. was additionally supported by a Graduate Education for Minorities (GEM) Fellowship, the University of Pennsylvania's Fontaine Fellowship, the Hispanic Scholarship Fund (HSF), and a Predoc to Postdoc Transition Award from the National Cancer Institute (NCI) (F99 CA2844294). R.P. was supported by a NIH Medical Scientist Training Program Grant (T32GM07170) and an NIH NHLBI F30 Fellowship (F30HL162465-01A1). M.J.M. was supported by a NIH Director's New Innovator Award (DP2 TR002776), a Burroughs Wellcome Fund Career Award at the Scientific Interface (CASI), the Cystic Fibrosis Foundation (MITCHE2410), an American Cancer Society Research Scholar Grant (RSG-22-122-01-ET), and an NSF CAREER Award (CBET-2145491). Data for this manuscript were generated using the Penn Cytomics and Cell Sorting Shared Resource Laboratory at the University of Pennsylvania and is partially supported by the Abramson Cancer Center NCI Grant (P30 016520, RRid:SCR 022376). We would also like to acknowledge Gitanjali Kaw for experimental assistance.

REFERENCES

(1) Hwang, W. Y.; Fu, Y.; Reyon, D.; Maeder, M. L.; Tsai, S. Q.; Sander, J. D.; Peterson, R. T.; Yeh, J.-R. J.; Joung, J. K. Efficient Genome Editing in Zebrafish Using a CRISPR-Cas System. *Nat. Biotechnol.* **2013**, *31* (3), 227–229.
(2) Cho, S. W.; Kim, S.; Kim, J. M.; Kim, J.-S. Targeted Genome Engineering in Human Cells with the Cas9 RNA-Guided Endonuclease. *Nat. Biotechnol.* **2013**, *31* (3), 230–232.

(3) Jinek, M.; East, A.; Cheng, A.; Lin, S.; Ma, E.; Doudna, J. RNA-Programmed Genome Editing in Human Cells. *Elife* **2013**, *2*, No. e00471.
(4) Cong, L.; Ran, F. A.; Cox, D.; Lin, S.; Barretto, R.; Habib, N.; Hsu, P. D.; Wu, X.; Jiang, W.; Marraffini, L. A.; Zhang, F. Multiplex Genome Engineering Using CRISPR/Cas Systems. *Science* **2013**, *339* (6121), 819–823.
(5) Mali, P.; Yang, L.; Esvelt, K. M.; Aach, J.; Guell, M.; DiCarlo, J. E.; Norville, J. E.; Church, G. M. RNA-Guided Human Genome Engineering via Cas9. *Science* **2013**, *339* (6121), 823–826.
(6) Gostimskaya, I. CRISPR–Cas9: A History of Its Discovery and Ethical Considerations of Its Use in Genome Editing. *Biochemistry* **2022**, *87* (8), 777–788.
(7) Wang, J. Y.; Doudna, J. A. CRISPR Technology: A Decade of Genome Editing Is Only the Beginning. *Science* **2023**, *379* (6629), No. eadd8643.
(8) Park, S. H.; Bao, G. CRISPR/Cas9 Gene Editing for Curing Sickle Cell Disease. *Transfus. Apher. Sci.* **2021**, *60* (1), 103060.
(9) Himič, V.; Davies, K. E. Evaluating the Potential of Novel Genetic Approaches for the Treatment of Duchenne Muscular Dystrophy. *Eur. J. Hum. Genet.* **2021**, *29* (9), 1369–1376.
(10) Choi, E.; Koo, T. CRISPR Technologies for the Treatment of Duchenne Muscular Dystrophy. *Mol. Ther.* **2021**, *29* (11), 3179–3191.
(11) Maule, G.; Arosio, D.; Cereseto, A. Gene Therapy for Cystic Fibrosis: Progress and Challenges of Genome Editing. *Int. J. Mol. Sci.* **2020**, *21* (11), 3903.
(12) Huang, D.; Miller, M.; Ashok, B.; Jain, S.; Peppas, N. A. CRISPR/Cas Systems to Overcome Challenges in Developing the next Generation of T Cells for Cancer Therapy. *Adv. Drug Delivery Rev.* **2020**, *158*, 17–35.
(13) Ferdosi, S. R.; Ewaisha, R.; Moghadam, F.; Krishna, S.; Park, J. G.; Ebrahimekhani, M. R.; Kiani, S.; Anderson, K. S. Multifunctional CRISPR-Cas9 with Engineered Immunosilenced Human T Cell Epitopes. *Nat. Commun.* **2019**, *10* (1), 1842.
(14) Jin, J.; Li, Y.; Deng, F.; Yang, L.; Lin, Y.; Yang, C.; Dai, W.; Zhang, H.; He, B.; Zhang, Q.; Wang, X. A Dual Gene Combination Therapy Approach by KRAS-G12V Gene Editing and SLC25A22 Gene Silencing for KRAS-Mutant Colorectal Cancer. *Nano Today* **2024**, *56*, 102291.
(15) Khirallah, J.; Eimbinder, M.; Li, Y.; Xu, Q. Clinical Progress in Genome-Editing Technology and in Vivo Delivery Techniques. *Trends Genet.* **2023**, *39* (3), 208–216.
(16) Shirley, J. L.; de Jong, Y. P.; Terhorst, C.; Herzog, R. W. Immune Responses to Viral Gene Therapy Vectors. *Mol. Ther.* **2020**, *28* (3), 709–722.
(17) Li, Y.; Bolinger, J.; Yu, Y.; Glass, Z.; Shi, N.; Yang, L.; Wang, M.; Xu, Q. Intracellular Delivery and Biodistribution Study of CRISPR/Cas9 Ribonucleoprotein Loaded Bioreducible Lipidoid Nanoparticles. *Biomater. Sci.* **2019**, *7* (2), 596–606.
(18) Walther, J.; Wilbie, D.; Tissingh, V. S. J.; Öktem, M.; van der Veen, H.; Lou, B.; Mastrobattista, E. Impact of Formulation Conditions on Lipid Nanoparticle Characteristics and Functional Delivery of CRISPR RNP for Gene Knock-Out and Correction. *Pharmaceutics* **2022**, *14* (1), 213.
(19) Zhang, X.; Li, B.; Luo, X.; Zhao, W.; Jiang, J.; Zhang, C.; Gao, M.; Chen, X.; Dong, Y. Biodegradable Amino-Ester Nanomaterials for Cas9mRNA Delivery in Vitro and in Vivo. *ACS Appl. Mater. Interfaces* **2017**, *9* (30), 25481–25487.
(20) Hajj, K. A.; Melamed, J. R.; Chaudhary, N.; Lamson, N. G.; Ball, R. L.; Yerneni, S. S.; Whitehead, K. A. A Potent Branched-Tail Lipid Nanoparticle Enables Multiplexed mRNA Delivery and Gene Editing In Vivo. *Nano Lett.* **2020**, *20* (7), 5167–5175.
(21) Cheng, Q.; Wei, T.; Farbiak, L.; Johnson, L. T.; Dilliard, S. A.; Siegwart, D. J. Selective Organ Targeting (SORT) Nanoparticles for Tissue-Specific mRNA Delivery and CRISPR–Cas Gene Editing. *Nat. Nanotechnol.* **2020**, *15* (4), 313–320.
(22) Li, B.; Manan, R. S.; Liang, S.-Q.; Gordon, A.; Jiang, A.; Varley, A.; Gao, G.; Langer, R.; Xue, W.; Anderson, D. Combinatorial Design

- of Nanoparticles for Pulmonary mRNA Delivery and Genome Editing. *Nat. Biotechnol.* **2023**, *41* (10), 1410–1415.
- (23) Piotrowski-Daspit, A. S.; Barone, C.; Lin, C.-Y.; Deng, Y.; Wu, D.; Binns, T. C.; Xu, E.; Ricciardi, A. S.; Putman, R.; Garrison, A.; Nguyen, R.; Gupta, A.; Fan, R.; Glazer, P. M.; Saltzman, W. M.; Egan, M. E. In Vivo Correction of Cystic Fibrosis Mediated by PNA Nanoparticles. *Sci. Adv.* **2022**, *8*, 40.
- (24) Hendel, A.; Bak, R. O.; Clark, J. T.; Kennedy, A. B.; Ryan, D. E.; Roy, S.; Steinfeld, L.; Lunstad, B. D.; Kaiser, R. J.; Wilkens, A. B.; Bacchetta, R.; Tsalenko, A.; Dellinger, D.; Bruhn, L.; Porteus, M. H. Chemically Modified Guide RNAs Enhance CRISPR-Cas Genome Editing in Human Primary Cells. *Nat. Biotechnol.* **2015**, *33* (9), 985–989.
- (25) Wei, T.; Cheng, Q.; Min, Y.-L.; Olson, E. N.; Siegwart, D. J. Systemic Nanoparticle Delivery of CRISPR-Cas9 Ribonucleoproteins for Effective Tissue Specific Genome Editing. *Nat. Commun.* **2020**, *11* (1), 3232.
- (26) van Haasteren, J.; Li, J.; Scheideler, O. J.; Murthy, N.; Schaffer, D. V. The Delivery Challenge: Fulfilling the Promise of Therapeutic Genome Editing. *Nat. Biotechnol.* **2020**, *38* (7), 845–855.
- (27) Mrksich, K.; Padilla, M. S.; Joseph, R. A.; Han, E. L.; Kim, D.; Palanki, R.; Xu, J.; Mitchell, M. J. Influence of Ionizable Lipid Tail Length on Lipid Nanoparticle Delivery of mRNA of Varying Length. *J. Biomed. Mater. Res.* **2024**, *112* (n/a), 1494–1505.
- (28) Onuma, H.; Sato, Y.; Harashima, H. Lipid Nanoparticle-Based Ribonucleoprotein Delivery for in Vivo Genome Editing. *J. Controlled Release* **2023**, *355*, 406–416.
- (29) Ho, T.-C.; Kim, H. S.; Chen, Y.; Li, Y.; LaMere, M. W.; Chen, C.; Wang, H.; Gong, J.; Palumbo, C. D.; Ashton, J. M.; et al. Scaffold-Mediated CRISPR-Cas9 Delivery System for Acute Myeloid Leukemia Therapy. *Sci. Adv.* **2021**, *7* (21), No. eabg3217.
- (30) Rui, Y.; Wilson, D. R.; Choi, J.; Varanasi, M.; Sanders, K.; Karlsson, J.; Lim, M.; Green, J. J. Carboxylated Branched Poly(β -Amino Ester) Nanoparticles Enable Robust Cytosolic Protein Delivery and CRISPR-Cas9 Gene Editing. *Sci. Adv.* **2019**, *5* (12), No. eaay3255.
- (31) Lee, B.; Lee, K.; Panda, S.; Gonzales-Rojas, R.; Chong, A.; Bugay, V.; Park, H. M.; Brenner, R.; Murthy, N.; Lee, H. Y. Nanoparticle Delivery of CRISPR into the Brain Rescues a Mouse Model of Fragile X Syndrome from Exaggerated Repetitive Behaviours. *Nat. Biomed. Eng.* **2018**, *2* (7), 497–507.
- (32) Lee, K.; Conboy, M.; Park, H. M.; Jiang, F.; Kim, H. J.; Dewitt, M. A.; Mackley, V. A.; Chang, K.; Rao, A.; Skinner, C.; Shobha, T.; Mehdipour, M.; Liu, H.; Huang, W.; Lan, F.; Bray, N. L.; Li, S.; Corn, J. E.; Kataoka, K.; Doudna, J. A.; Conboy, I.; Murthy, N. Nanoparticle Delivery of Cas9 Ribonucleoprotein and Donor DNA in Vivo Induces Homology-Directed DNA Repair. *Nat. Biomed. Eng.* **2017**, *1* (11), 889–901.
- (33) Garber, K. Alnylam Launches Era of RNAi Drugs. *Nat. Biotechnol.* **2018**, *36*, 777–778.
- (34) Polack, F. P.; Thomas, S. J.; Kitchin, N.; Absalon, J.; Gurtman, A.; Lockhart, S.; Perez, J. L.; Pérez Marc, G.; Moreira, E. D.; Zerbini, C.; Bailey, R.; Swanson, K. A.; Roychoudhury, S.; Koury, K.; Li, P.; Kalina, W. V.; Cooper, D.; Frenck, R. W.; Hammitt, L. L.; Türeci, Ö.; Nell, H.; Schaefer, A.; Ünal, S.; Tresnan, D. B.; Mather, S.; Dormitzer, P. R.; Şahin, U.; Jansen, K. U.; Gruber, W. C. Safety and Efficacy of the BNT162b2 mRNA COVID-19 Vaccine. *N. Engl. J. Med.* **2020**, *383* (27), 2603.
- (35) Baden, L. R.; El Sahly, H. M.; Essink, B.; Kotloff, K.; Frey, S.; Novak, R.; Diemert, D.; Spector, S. A.; Rouphael, N.; Creech, C. B.; McGettigan, J.; Khetan, S.; Segall, N.; Solis, J.; Brosz, A.; Fierro, C.; Schwartz, H.; Neuzil, K.; Corey, L.; Gilbert, P.; Janes, H.; Follmann, D.; Marovich, M.; Masciola, J.; Polakowski, L.; Ledgerwood, J.; Graham, B. S.; Bennett, H.; Pajon, R.; Knightly, C.; Leav, B.; Deng, W.; Zhou, H.; Han, S.; Ivarsson, M.; Miller, J.; Zaks, T. Efficacy and Safety of the mRNA-1273 SARS-CoV-2 Vaccine. *N. Engl. J. Med.* **2021**, *384* (5), 403.
- (36) Shepherd, S. J.; Warzecha, C. C.; Yadavali, S.; El-Mayta, R.; Alameh, M.-G.; Wang, L.; Weissman, D.; Wilson, J. M.; Issadore, D.; Mitchell, M. J. Scalable mRNA and siRNA Lipid Nanoparticle Production Using a Parallelized Microfluidic Device. *Nano Lett.* **2021**, *21* (13), 5671–5680.
- (37) Kulkarni, J. A.; Myhre, J. L.; Chen, S.; Tam, Y. Y. C.; Danescu, A.; Richman, J. M.; Cullis, P. R. Design of Lipid Nanoparticles for in Vitro and in Vivo Delivery of Plasmid DNA. *Nanomedicine* **2017**, *13* (4), 1377.
- (38) Zatsepin, T. S.; Kotelevtsev, Y. V.; Koteliansky, V. Lipid Nanoparticles for Targeted siRNA Delivery - Going from Bench to Bedside. *Int. J. Nanomed.* **2016**, *5*, 3077–86.
- (39) Swingle, K. L.; Hamilton, A. G.; Mitchell, M. J. Lipid Nanoparticle-Mediated Delivery of mRNA Therapeutics and Vaccines. *Trends Mol. Med.* **2021**, *27*, 616.
- (40) Chang, J.; Chen, X.; Glass, Z.; Gao, F.; Mao, L.; Wang, M.; Xu, Q. Integrating Combinatorial Lipid Nanoparticle and Chemically Modified Protein for Intracellular Delivery and Genome Editing. *Acc. Chem. Res.* **2019**, *52* (3), 665–675.
- (41) Wang, M.; Zuris, J. A.; Meng, F.; Rees, H.; Sun, S.; Deng, P.; Han, Y.; Gao, X.; Pouli, D.; Wu, Q.; Georgakoudi, I.; Liu, D. R.; Xu, Q. Efficient Delivery of Genome-Editing Proteins Using Bioreducible Lipid Nanoparticles. *Proc. Natl. Acad. Sci. U. S. A.* **2016**, *113* (11), 2868–2873.
- (42) Haley, R. M.; Chan, A.; Billingsley, M. M.; Gong, N.; Padilla, M. S.; Kim, E. H.; Wang, H.; Yin, D.; Wangenstein, K. J.; Tsourkas, A.; Mitchell, M. J. Lipid Nanoparticle Delivery of Small Proteins for Potent In Vivo RAS Inhibition. *ACS Appl. Mater. Interfaces* **2023**, *15* (18), 21877–21892.
- (43) Billingsley, M. M.; Singh, N.; Ravikumar, P.; Zhang, R.; June, C. H.; Mitchell, M. J. Ionizable Lipid Nanoparticle-Mediated mRNA Delivery for Human CAR T Cell Engineering. *Nano Lett.* **2020**, *20* (3), 1578–1589.
- (44) Chan, A.; Wang, H. H.; Haley, R. M.; Song, C.; Gonzalez-Martinez, D.; Bugaj, L.; Mitchell, M. J.; Tsourkas, A. Cytosolic Delivery of Small Protein Scaffolds Enables Efficient Inhibition of Ras and Myc. *Mol. Pharmaceutics* **2022**, *19* (4), 1104–1116.
- (45) Atsavaprane, E.; Haley, R. M.; Billingsley, M. M.; Chan, A.; Ruan, B.; Figueroa-Espada, C. G.; Gong, N.; Mukalel, A. J.; Bryan, P. N.; Mitchell, M. J. Ionizable Lipid Nanoparticles for RAS Protease Delivery to Inhibit Cancer Cell Proliferation. *J. Controlled Release* **2024**, *370*, 614–625.
- (46) Bhakta, S.; Sakari, M.; Tsukahara, T. RNA Editing of BFP, a Point Mutant of GFP, Using Artificial APOBEC1 Deaminase to Restore the Genetic Code. *Sci. Rep.* **2020**, *10* (1), 17304.
- (47) Glaser, A.; McColl, B.; Vadolas, J. GFP to BFP Conversion: A Versatile Assay for the Quantification of CRISPR/Cas9-Mediated Genome Editing. *Mol. Ther. Nucleic Acids* **2016**, *5*, No. e334.
- (48) El-Mayta, R.; Zhang, R.; Shepherd, S. J.; Wang, F.; Billingsley, M. M.; Dudkin, V.; Klein, D.; Lu, H. D.; Mitchell, M. J. A Nanoparticle Platform for Accelerated In Vivo Oral Delivery Screening of Nucleic Acids. *Adv. Ther.* **2021**, *4* (1), 2000111.
- (49) Omo-Lamai, S.; Zamora, M. E.; Patel, M. N.; Wu, J.; Nong, J.; Wang, Z.; Peshkova, A.; Majumder, A.; Melamed, J. R.; Chase, L. S.; et al. Physicochemical Targeting of Lipid Nanoparticles to the Lungs Induces Clotting: Mechanisms and Solutions. *Adv. Mater.* **2024**, *36* (26), 2312026.
- (50) Weber, J. A.; Lang, J. F.; Carrell, E. M.; Alameh, M.-G.; Davidson, B. L. Temporal Restriction of Cas9 Expression Improves CRISPR-Mediated Deletion Efficacy and Fidelity. *Mol. Ther. Nucleic Acids* **2024**, *35* (2), 102172.
- (51) Aimo, A.; Castiglione, V.; Rapezzi, C.; Franzini, M.; Panichella, G.; Vergaro, G.; Gillmore, J.; Fontana, M.; Passino, C.; Emdin, M. RNA-Targeting and Gene Editing Therapies for Transthyretin Amyloidosis. *Nat. Rev. Cardiol.* **2022**, *19* (10), 655–667.
- (52) Gillmore, J. D.; Gane, E.; Taubel, J.; Kao, J.; Fontana, M.; Maitland, M. L.; Seitzer, J.; O'Connell, D.; Walsh, K. R.; Wood, K.; Phillips, J.; Xu, Y.; Amaral, A.; Boyd, A. P.; Cehelsky, J. E.; McKee, M. D.; Schiermeier, A.; Harari, O.; Murphy, A.; Kyratsous, C. A.; Zambrowicz, B.; Soltys, R.; Gutstein, D. E.; Leonard, J.; Sepp-

Lorenzino, L.; Leibold, D. CRISPR-Cas9 In Vivo Gene Editing for Transthyretin Amyloidosis. *N. Engl. J. Med.* **2021**, *385* (6), 493–502.

(53) Chatterjee, S.; Kon, E.; Sharma, P.; Peer, D. Endosomal Escape: A Bottleneck for LNP-Mediated Therapeutics. *Proc. Natl. Acad. Sci. U. S. A.* **2024**, *121* (11), No. e2307800120.

(54) Zhang, L.; Button, B.; Gabriel, S. E.; Burkett, S.; Yan, Y.; Skiadopoulos, M. H.; Dang, Y. L.; Vogel, L. N.; McKay, T.; Mengos, A.; Boucher, R. C.; Collins, P. L.; Pickles, R. J. CFTR Delivery to 25% of Surface Epithelial Cells Restores Normal Rates of Mucus Transport to Human Cystic Fibrosis Airway Epithelium. *PLoS Biol.* **2009**, *7* (7), No. e1000155.

(55) Bulcaen, M.; Kortleven, P.; Liu, R. B.; Maule, G.; Dreano, E.; Kelly, M.; Ensinck, M. M.; Thierie, S.; Smits, M.; Ciciani, M.; Hatton, A.; Chevalier, B.; Ramalho, A. S.; Casadevall i Solvas, X.; Debyser, Z.; Vermeulen, F.; Gijsbers, R.; Sermet-Gaudelus, I.; Cereseto, A.; Carlon, M. S. Prime Editing Functionally Corrects Cystic Fibrosis-Causing CFTR Mutations in Human Organoids and Airway Epithelial Cells. *Cell Rep. Med.* **2024**, *5* (5), 101544.

(56) Yang, Y.; Wang, L.; Bell, P.; McMennamin, D.; He, Z.; White, J.; Yu, H.; Xu, C.; Morizono, H.; Musunuru, K.; Batshaw, M. L.; Wilson, J. M. A Dual AAV System Enables the Cas9-Mediated Correction of a Metabolic Liver Disease in Newborn Mice. *Nat. Biotechnol.* **2016**, *34* (3), 334–338.

(57) Riley, R. S.; Kashyap, M. V.; Billingsley, M. M.; White, B.; Alameh, M.-G.; Bose, S. K.; Zoltick, P. W.; Li, H.; Zhang, R.; Cheng, A. Y.; Weissman, D.; Peranteau, W. H.; Mitchell, M. J. Ionizable Lipid Nanoparticles for in Utero mRNA Delivery. *Sci. Adv.* **2021**, *7* (3), No. eaba1028.

(58) Brinkman, E. K.; Kousholt, A. N.; Harmsen, T.; Leemans, C.; Chen, T.; Jonkers, J.; van Steensel, B. Easy Quantification of Template-Directed CRISPR/Cas9 Editing. *Nucleic Acids Res.* **2018**, *46* (10), No. e58.

(59) Brinkman, E. K.; Chen, T.; Amendola, M.; van Steensel, B. Easy Quantitative Assessment of Genome Editing by Sequence Trace Decomposition. *Nucleic Acids Res.* **2014**, *42* (22), No. e168.

(60) Clement, K.; Rees, H.; Canver, M. C.; Gehrke, J. M.; Farouni, R.; Hsu, J. Y.; Cole, M. A.; Liu, D. R.; Joung, J. K.; Bauer, D. E.; Pinello, L. CRISPResso2 Provides Accurate and Rapid Genome Editing Sequence Analysis. *Nat. Biotechnol.* **2019**, *37* (3), 224–226.